Journal of Sound and Vibration 457 (2019) 213–226

Contents lists available at ScienceDirect

Journal of Sound and Vibration

journal homepage: www.elsevier.com/locate/jsvi

Experimentally measuring an isolated branch of Nonlinear normal modes

David A. Ehrhardt, Thomas L. Hill *, Simon A. Neild

Department of Mechanical Engineering, University of Bristol, Bristol BS8 1TR, UK

ARTICLE INFO

Article history:
Received 26 July 2018
Revised 17 April 2019
Accepted 6 June 2019
Available online 8 June 2019
Handling Editor: E Pavlovskaia

Keywords:
Nonlinear normal modes
Isolas
Experimental methods
Force appropriation
Phase-locking
Modal interactions

ABSTRACT

Nonlinear normal modes (NNMs) are a key tool for investigating the behaviour of nonlinear dynamic systems. Previous work has shown that branches of NNMs can be isolated from other NNM responses, in a similar manner to isolated, or *detached*, resonance curves in the forced responses. Their isolated nature poses a significant challenge for the prediction and measurement of these NNM branches. This paper illustrates how isolated NNMs may exist in two-degree-of-freedom systems, with cubic nonlinearities, that exhibit a 1:3 resonance. This is first introduced using a general two-mass oscillator, before considering a two-mode reduced-order model of a continuous *cross-beam* structure that exhibits a coupling between its primary bending and torsional modes. In both cases, a combination of analytical and numerical techniques is used to show how the isolated NNM branch may evolve from a set of bifurcating NNM branches. A nonlinear force appropriation technique is used to experimentally measure the NNMs of the cross-beam structure. By comparing these measurements to the numerical studies, it is shown that some of these NNMs are on the isolated branch, representing the first experimental confirmation of isolated NNM branches.

1. Introduction

When considering the responses of harmonically-forced nonlinear systems, it is well-known that multiple solutions can be observed at specific frequencies [1]. For certain systems, regions of forced responses are disconnected from other solutions [2–4]. These isolated regions, known as *isolated resonance curves*, *detached resonance curves* or *isolas*, have been observed experimentally in structures such as spring-mass systems [5,6] and beams [7]. As they are disconnected from the primary solution branches, these isolas prove challenging to compute, but often represent critical responses [8].

Nonlinear Normal Modes (NNMs) are used to interpret the responses of nonlinear systems and represent a nonlinear analogue of linear normal modes. NNMs were first defined by Rosenberg [9] and later expanded by Vakakis [10], Kerschen [11] and Haller [12]. These later works define an NNM as any periodic oscillation of the underlying conservative equations of motion – the definition that is used throughout the current paper. Numerous approaches for computing such NNMs have been proposed [13]. It has been shown that NNMs can be related to the forced responses of these systems using an energy-based method [14]. Of specific interest to the current work, the NNMs can be used to predict the onset of isolated resonance curves – as demonstrated in Refs. [3,15]. This approach requires that the NNM branches (i.e. the loci of NNM responses) of the system are known before the energy-based method is used to predict where the isolas cross the NNM branches.

* Corresponding author.
E-mail address: tom.hill@bristol.ac.uk (T.L. Hill).

https://doi.org/10.1016/j.jsv.2019.06.006

Along with isolated forced responses, nonlinear systems may exhibit isolated NNM branches – i.e. branches of periodic solutions of the underlying conservative system that are not connected to other branches, or to any zero-amplitude solutions. Note that this represents a modification to the definitions that consider NNMs to be extensions of the underlying linear responses, such as that by Shaw and Pierre [16,17]; however, as shown in this work, these NNM branches can correspond to significant features in the forced responses. Isolated NNM branches have received less attention than isolated forced responses and have yet to be observed experimentally. It is the existence of these isolated NNM branches, measured experimentally, that is the main subject of the current paper.

It has been theoretically shown that isolated NNM branches may exist in a mass-spring oscillator [15], and that these may evolve from non-isolated branches as the symmetry of the system is broken. In Ref. [15], the NNMs are computed analytically, and hence the isolated NNM branches are computed in the same manner as the primary branches. However, for more complex systems where analytical techniques are impractical, computing isolated NNM branches poses a significant challenge. This challenge is discussed in the current work, and it is shown that the isolated NNM branches may correspond to significant features in the forced responses.

Following on from Ref. [15], Section 2 of the current paper begins by showing that isolated NNM branches may exist in a simple two-mode system, representative of an asymmetric two-mass oscillator. This system exhibits a 1:3 resonance between the two modes (i.e. the second mode responds at three times the frequency of the first) and hence differs from the oscillator considered in Ref. [15] which exhibits a 1:1 resonance. It is then shown how this isolated NNM branch evolves from a set of bifurcating branches, as a nonlinear parameter of the system is varied, but the asymmetry is retained. These results, using a system that has been studied by numerous authors, provide a basis for interpreting the results presented in the remainder of the paper.

Section 3 introduces an experimental *cross-beam* structure, consisting of a clamped-clamped beam with an additional cross-beam that introduces a torsional component of vibration. The torsional mode is tuned such that this system also exhibits a 1:3 modal interaction. A similar structure has been considered in detail in Ref. [18]; however, the structure was tuned to exhibit a 1:1 resonance, and no isolated NNM branch was seen. In Section 3, a nonlinear reduced-order model is formulated using the implicit condensation method[1] [20,21], and it is shown that this model is equivalent to the simple two-mode system considered in Section 2. This model exhibits an isolated NNM branch, which is shown to evolve from a bifurcated set of branches as the symmetry of the structure is varied. Compared to the experimental realisation, this numerical model provides greater flexibility for investigating the dynamic behaviour of the structure, offering further context for the experimental results.

Finally, in Section 4, the NNMs of the structure are found experimentally using nonlinear force appropriation [22]. It is shown that there is a very good qualitative agreement between the experimentally-measured NNM branches, and those of the numerical reduced-order model. Not only are NNMs on an isolated branch measured experimentally, but it is shown that, for certain forcing amplitudes, responses on the isolated branch are inevitable and hence represent significant features of the response.

2. Isolated nonlinear normal modes in a two-mode system

In this section, isolated NNM branches are investigated using a two-mode system with cubic stiffness nonlinearities – arguably the simplest system that may exhibit isolated NNM branches. The system considered here is representative of an asymmetric two-mass oscillator, and in Section 3 it is shown that it may be extended to a continuous structure.

2.1. Computing nonlinear normal modes

The modal equations of motion of a two-mode system with cubic stiffness nonlinearities may be written

$$\ddot{\mathbf{q}} + \mathbf{\Lambda}\mathbf{q} + \mathbf{N}_q(\mathbf{q}) = \mathbf{0}\,, \tag{1}$$

with

$$\mathbf{q} = \begin{pmatrix} q_1 \\ q_2 \end{pmatrix}, \quad \mathbf{\Lambda} = \begin{bmatrix} \omega_1^2 & 0 \\ 0 & \omega_2^2 \end{bmatrix}, \quad \mathbf{N}_q = \begin{bmatrix} \gamma_1 q_1^3 + 3\gamma_2 q_1^2 q_2 + \gamma_3 q_1 q_2^2 + \gamma_4 q_2^3 \\ \gamma_2 q_1^3 + \gamma_3 q_1^2 q_2 + 3\gamma_4 q_1 q_2^2 + \gamma_5 q_2^3 \end{bmatrix}, \tag{2}$$

where q_i and ω_{ni} are the displacement and linear natural frequency of the ith mode, and where γ_i are nonlinear parameters. Note that γ_2, γ_3 and γ_4 appear in both equations of motion. The form of these coupling terms arises in the derivation of these equations of motion using Lagrange's equations – see Appendix A.

The natural frequencies and nonlinear parameters considered in this section are given in Table 1. These are representative of an asymmetric two-mass oscillator with cubic nonlinear springs, as described in Appendix B, where the physical parameters of the system are also provided.

The harmonic balance method is now used to compute the NNM branches, i.e. the branches of periodic solutions, of this system. The application of this is discussed briefly here, but readers are referred to Ref. [18], where the harmonic balance

[1] Note that numerous other reduced-order modelling techniques are available, [19].

Table 1
The modal parameters, shown to four significant figures.

ω_1 [rads^{-1}]	ω_2	γ_1 ($\times 10^{-2}$)	γ_2	γ_3	γ_4	γ_5
0.3121	1.026	21.49	−2.819	6.427	−0.1122	42.22

method is applied to a similar system, for further details. To apply the method, the ratio between the response frequencies of the two modes must first be assumed. As the ratio between the linear natural frequencies is approximately 1:3, i.e. $\omega_2/\omega_1 \approx 3$, it is assumed that the second mode, q_2, responds at three times the frequency of the first mode, q_1, i.e.

$$q_1 \approx U_1 \cos\left(\Omega t - \phi_1\right), \qquad q_2 \approx U_2 \cos\left(3\Omega t - \phi_2\right), \tag{3}$$

where U_i and ϕ_i are the amplitude and phase of the ith mode respectively, and where Ω is the response frequency of the first mode (such that the response frequency of the second mode is 3Ω). Note that the phases are included here to allow for a relative phase-difference between the modes – see Ref. [23] for further details.

The assumed solutions, Eq. (3), are then substituted into the modal equations of motion, Eq. (1). Next, the first and second equations are balanced for the terms responding at frequencies Ω and 3Ω respectively. This leads to the frequency-amplitude relationships of the NNMs, defined as

$$4\left(\omega_1^2 - \Omega^2\right)U_1 + 3\gamma_1 U_1^3 + p3\gamma_2 U_1^2 U_2 + 2\gamma_3 U_1 U_2^2 = 0, \tag{4a}$$

$$4\left(\omega_2^2 - 9\Omega^2\right)U_2 + p\gamma_2 U_1^3 + 2\gamma_3 U_1^2 U_2 + 3\gamma_5 U_2^3 = 0, \tag{4b}$$

where the parameter p denotes the phase difference between the two modes such that

$$p = \begin{cases} +1 & \text{when: } \phi_1 - \phi_2 = 0, \quad \text{i.e. the modes are in} - \text{phase,} \\ -1 & \text{when: } \phi_1 - \phi_2 = \pi, \quad \text{i.e. the modes are in antiphase.} \end{cases} \tag{5}$$

Note that the terms containing γ_4 do not lead to any resonant terms, and hence are not present in Eq. (4). The time-independent polynomial expressions, Eq. (4), can then be solved to find the response amplitudes, U_1 and U_2, in terms of the response frequency, Ω. See Ref. [18], where the solutions to a similar set of expressions are found, for further details.

Fig. 1 shows the NNM branches of the two-mode system, computed using the harmonic balance method. In Panels (*a–c*), the dark-blue lines represent the NNMs where the modes are in-phase, i.e. where $p = +1$, and the light-blue lines represent the antiphase NNMs, i.e. where $p = -1$. These are shown in terms of the initial displacements of the modes, $q_1(0)$ and $q_2(0)$, where the initial displacement of q_1 is defined as its maximum positive value. As such, when the two modes are in-phase the initial displacement of the second mode, $q_2(0)$, is positive, whilst an antiphase response gives a negative $q_2(0)$ value.

Although Panel (*b*) appears to show the in-phase and antiphase NNM branches crossing, the 3-D plot in Panel (*a*) reveals that this is due to the projection and, in fact, the antiphase NNM branch is isolated. This illustrates that, for the parameters considered here, an isolated NNM branch does exist in a simple two-mode system, with cubic stiffness terms, and a 1:3 resonance between the underlying linear modes.

Panels (*d–g*) show four different NNM responses in the projection of time against the modal amplitudes, $q_1(t)$ and $q_2(t)$. These illustrate how the phase between the two modes changes between the in-phase (dark blue) branch, shown in (*d*) and (*e*), and the antiphase (light blue) branch, shown in (*f*) and (*g*).

Note that additional NNM branches may exist for this system. For example, the primary branch emerging from the second linear natural frequency, which can be found using the harmonic balance method by setting the frequency ratio of the assumed solutions, Eq. (3), to 1:1. Furthermore, the NNMs are not necessarily limited to cases where the modes are in-phase or in antiphase, and additional phase relationships may exist [23]; however, the behaviour of interest here is captured by these phase relationships, hence the current study is limited to these cases.

2.2. Evolution of an isolated nonlinear normal mode from a bifurcation

In Ref. [15] it is shown that a two-mass oscillator may exhibit an isolated NNM branch with a 1:1 resonance between the modes. This 1:1 branch is shown to evolve from a set of NNM branches, of a symmetric system, that exhibit a bifurcation. By breaking this symmetry, an *imperfect* bifurcation is formed, i.e. the bifurcation connecting the two branches splits to form two separate, disconnected, branches, one of which is an isolated NNM branch [24]. It is now shown that the 1:3 isolated NNM branch, presented in Fig. 1, can also evolve from a set of bifurcating NNM branches, as this bifurcation becomes *imperfect*. Here, however, it is shown that this is not due to a symmetry-breaking of the system, and response may also exhibit a bifurcation when the system is asymmetric.

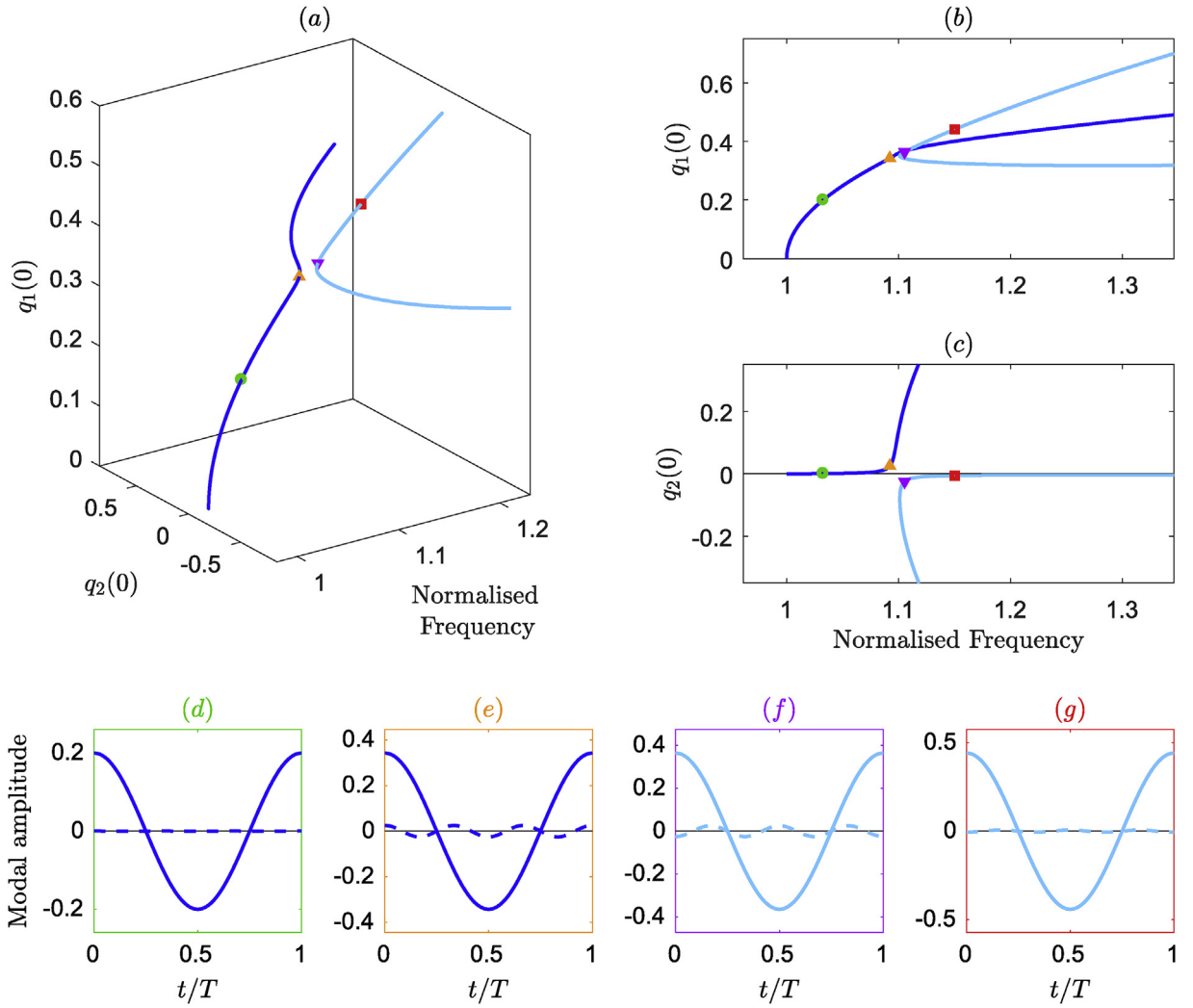

Fig. 1. The NNM branches, found using the harmonic balance method, of the two-mode system. Panel (*a*) is in the 3-D projection of response frequency normalised to the first linear natural frequency, i.e. Ω/ω_1, against the initial displacements of the first and second modes, $q_1(0)$ and $q_2(0)$. Panels (*b*) and (*c*) show the projection of normalised response frequency against the initial displacements of the first and second modes respectively. The light- and dark-blue lines represent the NNM branches where the linear modes are in-phase and antiphase respectively. The four coloured markers in Panels (*a–c*) correspond to four specific NNM responses. These responses are shown, parameterised in time, in Panels (*d–g*), which are in the projection of time, t (normalised to the period, T) against the modal displacement. The solid and dashed lines represent the first and second modal displacements, $q_1(t)$ and $q_2(t)$, respectively. (For interpretation of the references to colour in this figure legend, the reader is referred to the Web version of this article.)

The bifurcation between the NNM branches in Ref. [15] represents a transition between a single-mode NNM branch (i.e. NNMs composed of only the first mode) and a multi-mode NNM branch (i.e. NNMs composed of both modes). The single-mode NNM requires that the first mode can exist independently of the second mode, i.e. that $U_1 \neq 0$ and $U_2 = 0$, at certain amplitude levels. This may be achieved by setting $\gamma_2 = 0$, such that Eq. (4) become

$$\left[4\left(\omega_1^2 - \Omega^2\right) + 3\gamma_1 U_1^2 + 2\gamma_3 U_2^2\right] U_1 = 0\,, \tag{6a}$$

$$\left[4\left(\omega_2^2 - 9\Omega^2\right) + 2\gamma_3 U_1^2 + 3\gamma_5 U_2^2\right] U_2 = 0\,. \tag{6b}$$

Note that Eq. (6) also allow for solutions where both modes coexist and interact. This suggests that when $\gamma_2 = 0$, the system may exhibit a bifurcating set of NNM branches.

The nonlinear parameter γ_2 may be set to zero by varying the physical parameters of the two-mass oscillator represented by this model, as detailed in Appendix C. Here, the nonlinear parameter of the spring connecting the masses, α_2, is varied such that $\gamma_2 = 0$. This leads to the modal parameters given in Table 2, where $\alpha_2 = \alpha_{2,I}$ denotes the value of α_2 used previously,

Table 2
The modal parameters for the case when $\alpha_2 = \alpha_{2,I}$ (as shown previously in Table 1), and when $\alpha_2 = \alpha_{2,B}$. These are shown to four significant figures.

	ω_1 [rads^{-1}]	ω_2	γ_1 ($\times 10^{-2}$)	γ_2	γ_3	γ_4	γ_5
$\alpha_2 = \alpha_{2,I} = 0.02$	0.3121	1.026	21.49	−2.819	6.427	−0.1122	42.22
$\alpha_2 = \alpha_{2,B} \approx -0.01166$	0.3121	1.026	18.96	0.0	−2.967	3.366	38.36

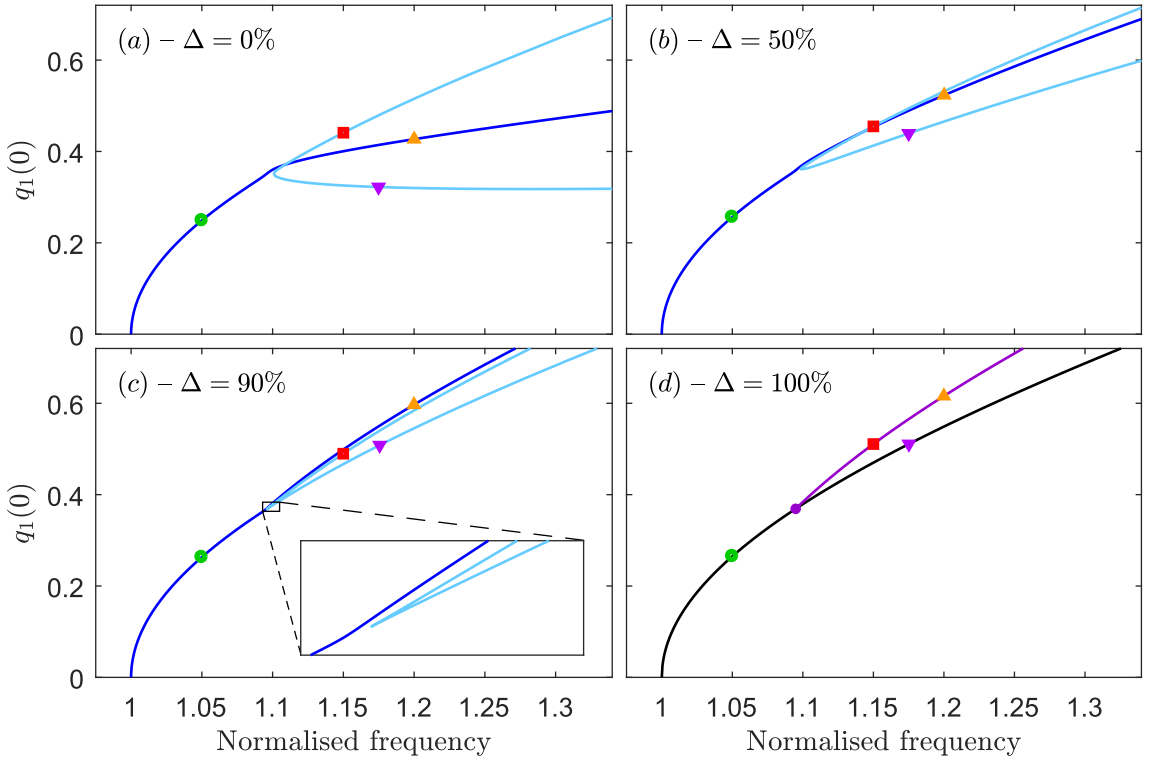

Fig. 2. The NNM branches, found using the harmonic balance method, of the two-mode system as the nonlinear parameter α_2 is varied. All four panels are shown in the projection of normalised response frequency against the initial displacement of the first mode, $q_1(0)$. Panel (*a*) shows the case where $\alpha_2 = \alpha_{2,I}$. Panels (*b*) and (*c*) then show the evolution of the NNM branches as α_2 approaches $\alpha_{2,B}$, and Panel (*d*) shows the case where $\alpha_2 = \alpha_{2,B}$. Panels (*a*–*c*) show the in-phase and antiphase NNM branches as dark- and light-blue lines respectively. The black and purple lines in Panel (*d*) show the single- and multi-mode NNM branches respectively, and the purple dot represents the bifurcation point. In all Panels, four markers are used to show the evolution of the branches. (For interpretation of the references to colour in this figure legend, the reader is referred to the Web version of this article.)

and $\alpha_2 = \alpha_{2,B}$ denotes the value that gives $\gamma_2 = 0$. Note that $\alpha_{2,I}$ is positive, hence corresponding to a spring with a hardening nonlinearity, whilst $\alpha_{2,B}$ is negative, hence corresponding to a spring with a softening nonlinearity.

Fig. 2 shows the evolution of the NNM branches as α_2 is varied from $\alpha_{2,I}$ to $\alpha_{2,B}$. This uses the parameter Δ, where $\alpha_2 = \alpha_{2,I} + \Delta\left(\alpha_{2,B} - \alpha_{2,I}\right)$. The case where $\Delta = 0\%$, and hence $\alpha_2 = \alpha_{2,I}$, is shown in Fig. 2(*a*) (and shown previously in Fig. 1(*b*)). The four coloured markers, that are fixed in frequency, are used to track four points on the NNM branches as they evolve. Fig. 2(*b*) shows the case where $\Delta = 50\%$ – i.e. α_2 is half-way between $\alpha_{2,I}$ and $\alpha_{2,B}$. In comparison to Fig. 2(*a*), it can be seen that the upper portion of the primary branch (dark-blue, with an orange triangle) has risen in amplitude, along with the lower portion of the isolated branch (light-blue, with a purple triangle). Little movement is seen in the lower portion of the primary branch (green circle), or the upper portion of the isolated branch (red square).

The case where $\Delta = 90\%$ is shown in Fig. 2(*c*). Again, this shows little movement in the lower portion of the primary branch (green circle), or the upper portion of the isolated branch (red square); however, the upper portion of the primary branch (orange triangle) has now moved above the isolated branch (red square). A detailed region shows that the antiphase (light-blue) NNM is still isolated.

Finally, the case where $\Delta = 100\%$, representing $\alpha_2 = \alpha_{2,B}$, is shown in Fig. 2(*d*). In this Panel, the black line represents NNMs that only contain the first mode, and the purple line represents NNMs containing both modes. The purple dot represents the bifurcation between these two branches, hence connecting the mixed-mode (purple), to the single-mode (black) NNM

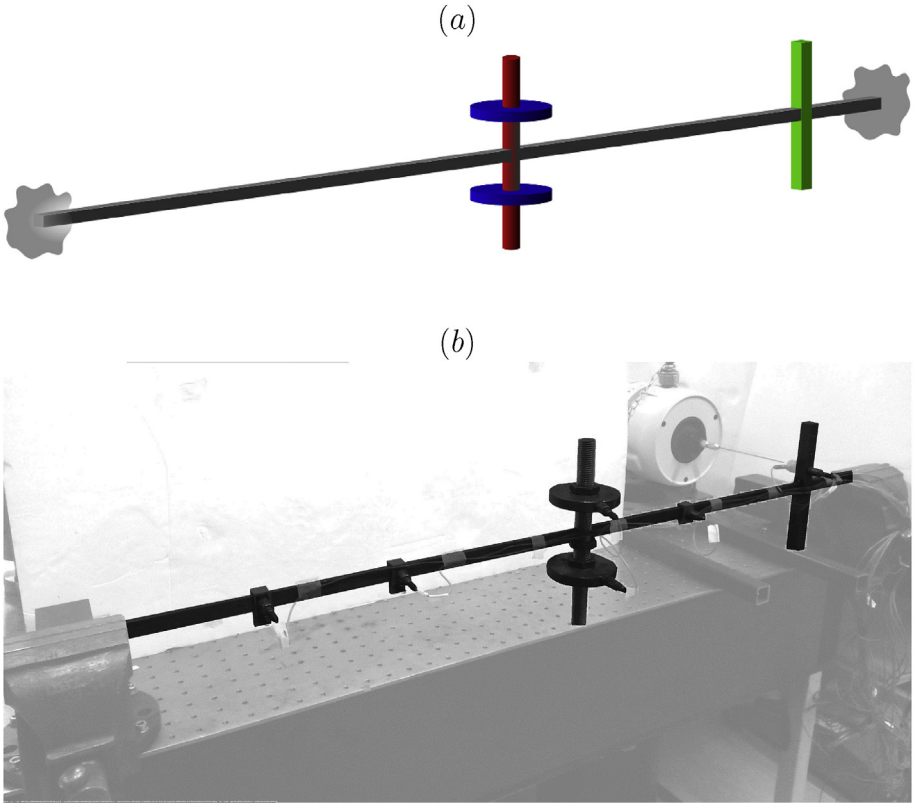

Fig. 3. The cross-beam structure considered in this paper. Panel (*a*) shows a schematic of the cross-beam, where the shaded regions at the ends of the main beam represent the clamped boundary conditions. Panel (*b*) shows a picture of the experimental realisation of the structure.

branch. As such, the mixed-mode branch is not isolated. Comparing Panel (*d*) to Panels (*a*–*c*), it can be seen that the upper portions of the primary and isolated branches (orange triangle and red square, respectively) have merged to form the multi-mode (purple) branch, whilst the single-mode (black) branch is composed of the lower portion of the isolated branch (purple triangle). This shows that the 1:3 isolated NNM branches can evolve from a set of bifurcating branches and represents an imperfect bifurcation. The physical system considered here is asymmetric for all configurations represented in Fig. 2, and hence this evolution is not driven by a breaking of the symmetry of the physical system.

2.3. Phase-locking in the NNM branches

In Fig. 2(*d*), the multi-mode branch is shown in purple (rather than light- or dark-blue, as previously) as the phase between the modes cannot be determined. This is due to the lack of phase-dependent terms in Eq. (6); i.e. Eq. (6) do not contain the phase-difference parameter p (defined in Eq. (5)). As such, the multi-mode branch is *phase-unlocked* [25]. As described in Ref. [26], phase-unlocked NNMs do not strongly attract forced responses; hence, it is not anticipated that a forced response following the single-mode branch would bifurcate and follow the multi-mode branch [25].

If a small γ_2 were introduced (such as in Fig. 2(*c*)) the phase of the backbone curves can once again be specified. However, a sufficiently small γ_2 will not significantly alter the structure of the system, and the phase-dependent terms in Eq. (6) will remain small, hence it can be assumed that the phase-locking mechanism will be weak. This suggests that a forced response following the lower portion of the primary NNM branch (green circles in Fig. 2) will not be strongly attracted to the upper portion of the primary branch (orange triangle), or the upper portion of the isolated branch (red square), as both of these are closely-related to a phase-unlocked solution. It therefore follows that we expect a forced response to be drawn to the lower portion of the isolated branch (purple triangle), despite its isolated nature. This concept is revisited in Section 4, where experimental results are discussed.

3. Isolated nonlinear normal modes in a continuous structure

Fig. 2 illustrates how isolated NNM branches may evolve from a set of bifurcating branches in a simple, two-mode system that is representative of a two-mass oscillator. In this section it is observed that a similar two-mode model, which exhibits

Table 3
The parameters of the nonlinear reduced-order models for the symmetric and asymmetric configurations of the cross-beam structure. These are shown to four significant figures.

	ω_1 [rads^{-1}]	ω_2	γ_1 ($\times 10^3$)	γ_2	γ_3	γ_4	γ_5
Symmetric	78.873	247.042	3625	0	800.0	0	7250
Asymmetric	78.860	247.614	3655	−214.3	849.6	−3.020	6849

isolated NNM branches, may be used to describe a continuous structure. It is shown that these isolated branches evolve from a set of bifurcating branches as the symmetry of the structure is changed.

3.1. A nonlinear cross-beam structure

The *cross-beam* structure, considered for the remainder of this paper, is illustrated in Fig. 3, where Panel (*a*) shows a schematic of the structure and Panel (*b*) shows an experimental realisation. This section is dedicated to numerical analysis of this structure, whilst experimental results are considered in Section 4. The structure consists of a 960 mm long rectangular beam, clamped at both ends, with two cross-beams. The circular cross-beam, shown in red in Fig. 3(*a*), is of length 220 mm and has two adjustable masses, shown in blue, that may be moved along the length of the cross-beam. The rectangular cross-beam, shown in green in Fig. 3(*a*), is used as a means of applying a torsional force in an experiment.

Adjusting the movable masses allows the natural frequencies of the structure to be tuned and allows its symmetry to be adjusted. When the structure is symmetric, its first two modes consist of a flexural bending of the main beam, and a torsional motion. If the masses are moved to break the symmetry, these modes change such that a small torsional component is introduced to the bending-dominated mode, and a small bending component is introduced to the torsion-dominated mode.

Further details about this structure, and how it may be tuned, can be found in Ref. [18]. Note that the structure described in Ref. [18] is a modified version of that shown in Fig. 3, where the natural frequencies of the bending and torsion modes are approximately equal; as such the structure exhibits a 1:1 resonance. However, here, the masses are tuned such that the natural frequency of the torsion-dominated mode is approximately three times that of the bending-dominated mode. As such, this structure exhibits a 1:3 resonance (as seen in the two-mass oscillator considered in Section 2). Details of the experimental procedure are given later in Section 4.

When the cross-beam structure undergoes large deflections, the axial stretching along the length of the main beam leads to a nonlinear stiffening effect. To capture the effect of this nonlinearity on the bending- and torsion-dominated modes, a two-mode nonlinear reduced-order model (ROM) is derived using the implicit condensation and expansion method (ICE), as described in Refs. [20,21]. The ICE method captures the nonlinear coupling between these two modes and any membrane-type modes, described in a finite-element model of the structure. Here, this finite-element model has been constructed using ABAQUS® and consists of a total of 288 B31 beam elements (with 6 DOFs at each node [27]). Additionally, linear axial springs are added to mimic the boundary conditions, as statically measured in Ref. [18]. Note that the finite-element model has not been updated to match the experimental results; however, the model is sufficiently close that the same qualitative behaviour is seen – as discussed later in Section 4. The ICE method generates a ROM described by equations of motion that are identical in form[2] to the two-mode equations of motion considered in Section 2 – Eq. (1).

Two different configurations of the structure are considered in this paper: one in which the masses are arranged symmetrically, and one in which they are asymmetric. The resulting values of the parameters of the nonlinear ROM are given in Table 3. Note that the asymmetric case has been tuned such that the linear natural frequencies, ω_1 and ω_2, are approximately equal to the symmetric case (and retaining an approximate 1:3 ratio). Due to the approximate nature of the ICE method, the symmetric case cannot be precisely represented by the ROM. However, near symmetry the nonlinear parameters γ_2 and γ_4 are close to zero, relative to γ_1, γ_3 and γ_5; as such, they have artificially been set to zero in Table 3 to reflect the *truly* symmetric case. Note that the parameters of the symmetric configuration are comparable to those of the two-mode system for the case where $\alpha_2 = \alpha_{2,B}$, shown in Table 2; however, for the cross-beam structure, γ_4 is also equal to zero.

The NNM branches of the nonlinear ROMs are computed using the numerical continuation algorithm NNMcont [28]. Unlike the harmonic balance method, used in Section 2, this numerical approach does not require an assumed form of the response, and thus is expected to give greater accuracy. However, the disadvantage of numerical continuation is that it requires an initial solution to compute an NNM branch. For a primary NNM branch, this solution may simply be the low-amplitude linear solution [28]; however, the isolated NNM branches require an NNM that is outside of the linear regime for an initial solution. Here, the harmonic balance method is used to compute approximate NNMs on the isolated branch. One of these approximate solutions is then used as an initial solution for continuation. This combination of both techniques ensures that all relevant NNM branches are computed to a high degree of accuracy [15].

[2] The ICE method also generates quadratic nonlinear terms; however, these are much smaller than the cubic terms and so have been neglected.

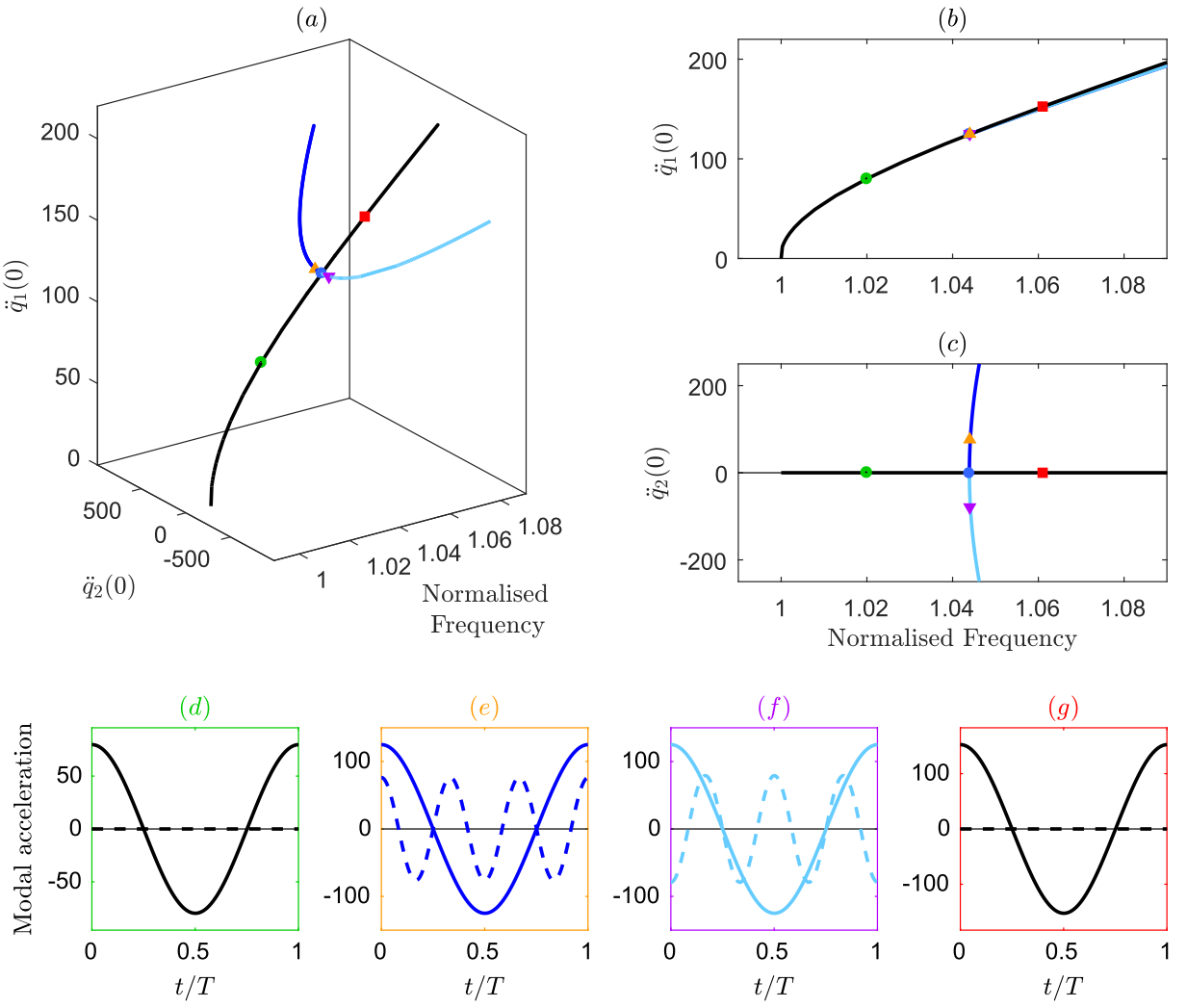

Fig. 4. The NNM branches for the ROM of the symmetric cross-beam. Panel (*a*) is in the 3-D projection of normalised response frequency against the initial acceleration of the first and second modes, $\ddot{q}_1(0)$ and $\ddot{q}_2(0)$. Panels (*b*) and (*c*) show the projection of normalised response frequency against $\ddot{q}_1(0)$ and $\ddot{q}_2(0)$ respectively. In these three panels, the black, dark-blue and light-blue lines represent the single-mode, in-phase and antiphase NNM branches respectively, and a blue dot marks the bifurcation between these branches. The four coloured markers in Panels (*a*–*c*) correspond to four specific NNM responses. These responses are shown, parameterised in time, in Panels (*d*–*g*), which are in the projection of time, t (normalised to the period, T) against the modal acceleration. The solid and dashed lines represent the first and second modal accelerations, $\ddot{q}_1$ and $\ddot{q}_2$, respectively. (For interpretation of the references to colour in this figure legend, the reader is referred to the Web version of this article.)

3.2. Responses of the cross-beam structure

The NNM branches of the symmetric ROM are shown in Fig. 4. Panels (*a*–*c*) show the normalised response frequency against the initial accelerations of the two modes.[3] The black line, shown in Panels (*a*–*c*) represents the NNMs consisting of a response in just the first linear mode. This is analogous to the black line shown for the bifurcating case in the two-mode system, Fig. 2(*c*). The dark- and light-blue lines represent NNMs containing both modes, which is analogous to the purple line[4] shown in Fig. 2(*c*). A blue dot in Fig. 2(*a*–*c*) denotes the pitchfork-like bifurcation that connects these two branches to the primary branch [29] – as such, these branches are not isolated.

The four coloured markers denote specific NNMs, whose time-parameterised responses are shown in Fig. 4(*d*–*g*). The Panels (*e*) and (*f*) show that this system exhibits a 1:3 resonance between the two modes when they interact, and that this may occur in-phase (the orange triangle and Panel (*e*)) or in antiphase (the purple triangle and Panel (*f*)). As previously, the two multi-mode

[3] Acceleration, rather than displacement, is used here to allow for easier comparison with experimental data in Section 4.

[4] Unlike the purple line in Fig. 2(*c*) (computed using the harmonic balance method) the phase between the two modes may be defined in Fig. 4 (computed using numerical continuation). This is due to the phase-locking between the harmonics of the modes, which are computed by the numerical solvers, hence allowing the phase to be defined. See Ref. [26] for further details.

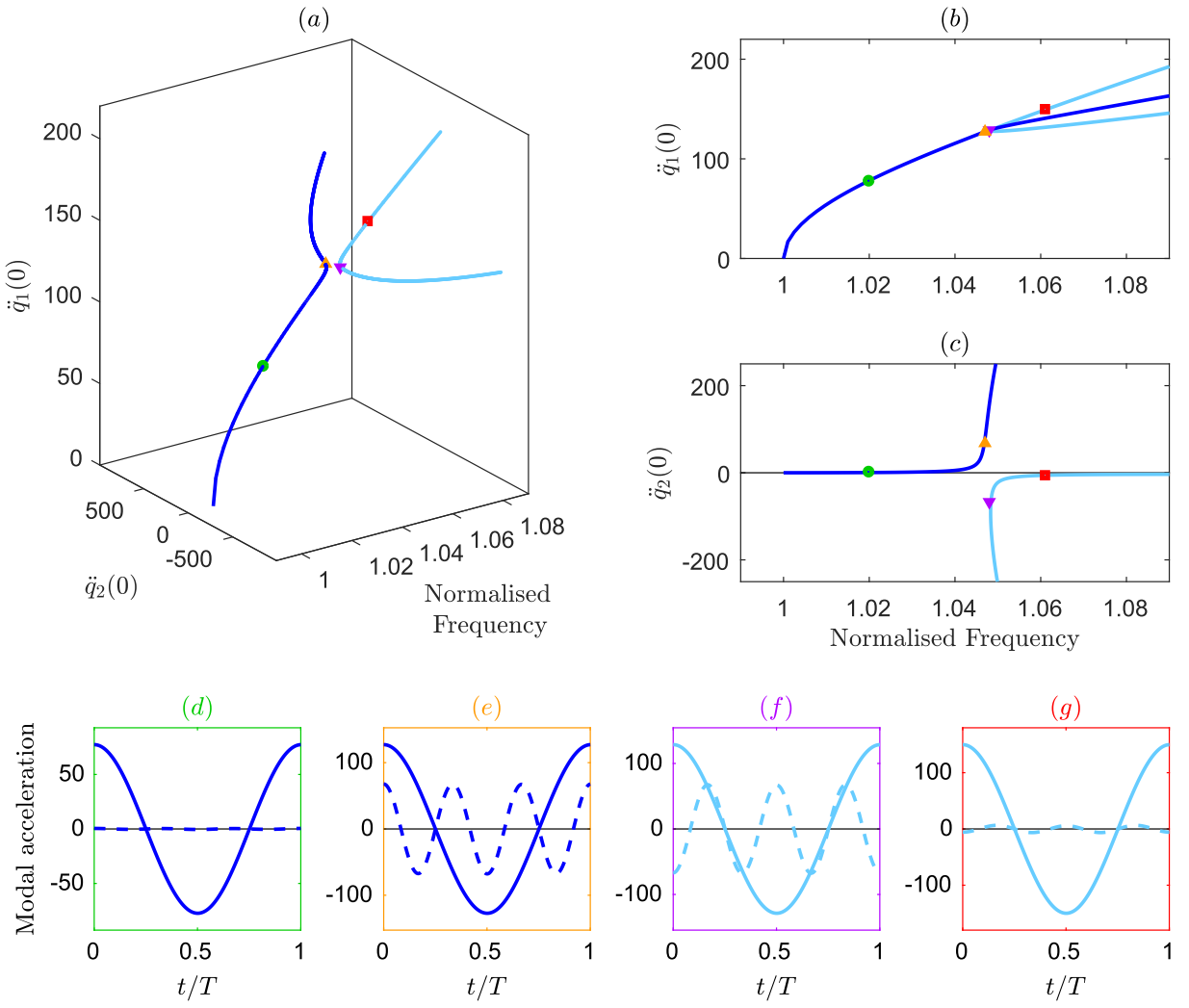

Fig. 5. The NNM branches for the ROM of the asymmetric cross-beam. Panel (*a*) is in the 3-D projection of normalised response frequency against the initial acceleration of the first and second modes. Panel (*b*) shows the projection of normalised response frequency against the initial acceleration of the first mode, and Panel (*c*) shows the normalised response frequency against the initial acceleration of the second mode. In these three panels, the dark- and light-blue lines represent the in-phase and antiphase NNM branches respectively. The four coloured markers in Panels (*a*–*c*) correspond to four specific NNM responses which are shown, parameterised in time, in Panels (*d*–*g*). Panels (*d*–*g*) are in the projection of time, *t* (normalised to the period, *T*) against modal acceleration. The solid and dashed lines represent the first and second modal accelerations, $\ddot{q}_1$ and $\ddot{q}_2$, respectively. (For interpretation of the references to colour in this figure legend, the reader is referred to the Web version of this article.)

NNM branches have positive $\ddot{q}_2(0)$ values when the two modes are in-phase (dark-blue), and negative $\ddot{q}_2(0)$ values when the two modes are in antiphase (light-blue). If a projection that did not reveal phase (such as maximum absolute amplitude) where used, these two branches would be superimposed [29].

Fig. 5 shows the NNM branches of the asymmetric configuration of the cross-beam structure. As with the symmetric case in Fig. 4, Panels (*a*–*c*) show the normalised response frequency against the initial acceleration of the two modes. The dark- and light-blue lines in Panels (*a*–*c*) represent the in-phase and antiphase NNM branches respectively. As previously, an antiphase response leads to a negative $\ddot{q}_2(0)$ value, and the time-parameterised NNMs in Panels (*d*–*g*) clearly show these phase differences. These time-series plots also show that these NNMs exhibit a 1:3 resonance.

Fig. 5 clearly shows that the antiphase (light-blue) NNM branch is isolated, showing that isolated NNM branches may exist in a conceptually-simple, continuous structure. Comparing Figs. 4 and 5 it can be seen that the isolated NNM branch arises from the breaking of the pitchfork-like bifurcation, to form an imperfect bifurcation. This is analogous to the evolution of the isolated NNM branch of the two-mode system, shown in Fig. 2.

As discussed previously, a known solution on the isolated branch has been used to initiate the continuation, which has been computed using the harmonic balance method. If a continuation scheme was initiated on the primary (in-phase) branch, without *a priori* knowledge of the existence of the isolated branch, it is unlikely its presence would be detected. Additionally, the isolated NNM branch is only connected to the primary branch when the system is purely symmetric. This is a special case, which

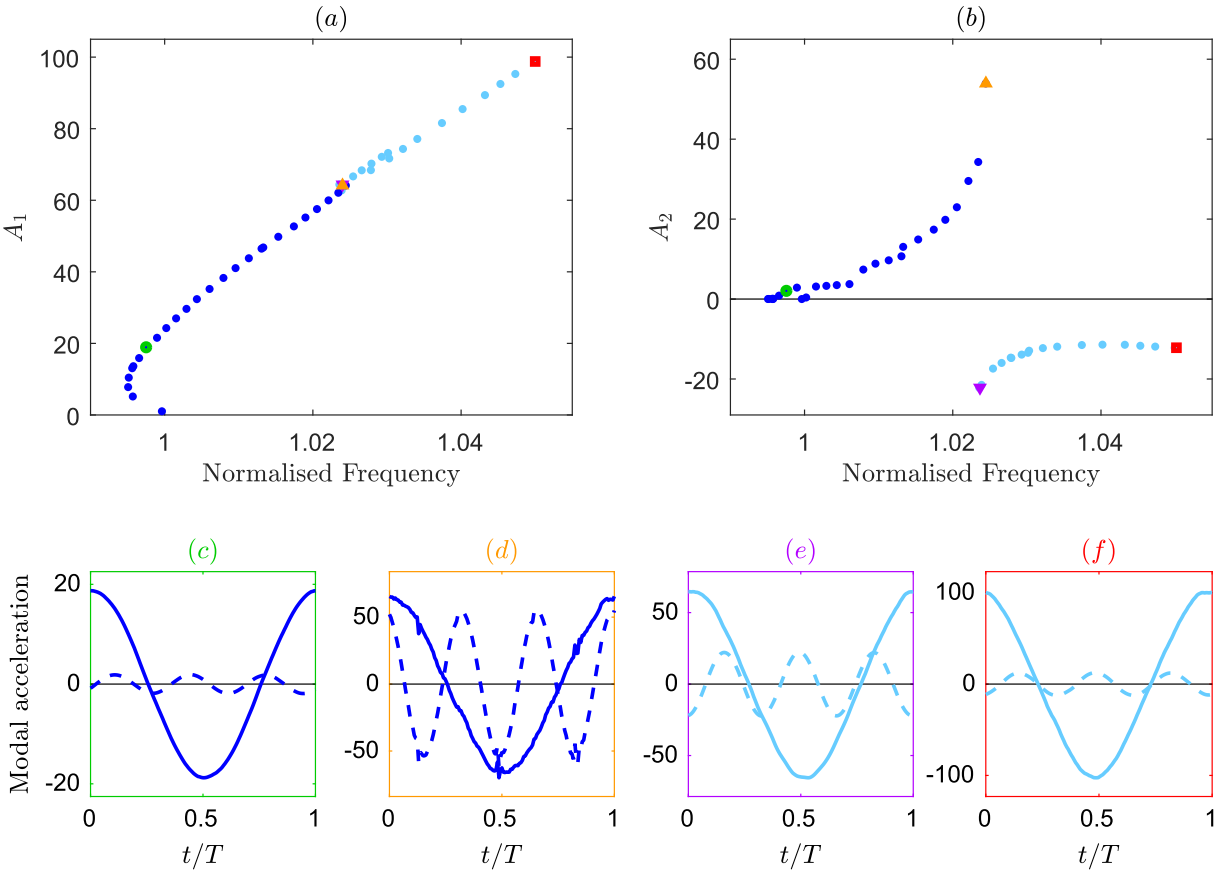

Fig. 6. The experimentally-measured responses of the asymmetric cross-beam structure. Panel (*a*) is in the projection of the normalised response frequency against the amplitude of acceleration of the first mode, A_1. Similarly, panel (*b*) is in the projection of the normalised response frequency against amplitude of acceleration of the second mode, A_2. In these two panels, the dark- and light-blue dots represent the in-phase and antiphase responses respectively. The four coloured markers in Panels (*a*) and (*b*) correspond to four specific responses which are shown, in the projection of time (normalised to the period of the response, T) against the modal acceleration, in Panels (*c–f*). The solid and dashed lines represent the first and second modal accelerations, $\ddot{q}_1$ and $\ddot{q}_2$, respectively. (For interpretation of the references to colour in this figure legend, the reader is referred to the Web version of this article.)

could not be found precisely using the parameters from the ICE method, due to its approximate nature, further complicating any attempt to find the isolated branch by continuation.

4. Experimental measurement of NNM branches

This section considers an experimental realisation of the cross-beam structure introduced in Section 3.1. A brief overview of the experimental procedure is provided before results are shown. For further details of the experimental procedure see Ref. [18].

4.1. Nonlinear experimental structure

The experimental realisation of the cross-beam structure was shown previously in Fig. 3(*b*). It can be seen that a shaker is attached to the rectangular cross-beam – shown in green in the schematic in Fig. 3(*a*). As the shaker is offset from centreline of the main beam, this provides a small torsional component of excitation. Six accelerometers are attached to the structure to measure its dynamic response and the excitation force is measured using a force transducer.

The adjustable masses, shown in blue in Fig. 3(*a*), are tuned such that the ratio between the linear natural frequencies is slightly higher than 1:3 (measured as 1:3.09, with the bending-dominated mode at the lower frequency). Note that if the ratio is less than 1:3, the isolated NNM branch will not be seen.[5] The masses are also positioned slightly asymmetrically, i.e. they are

[5] Note that this is not the case for all systems – for example in Ref. [15] an isolated NNM branch is seen in a system exhibiting a 1:1 resonance.

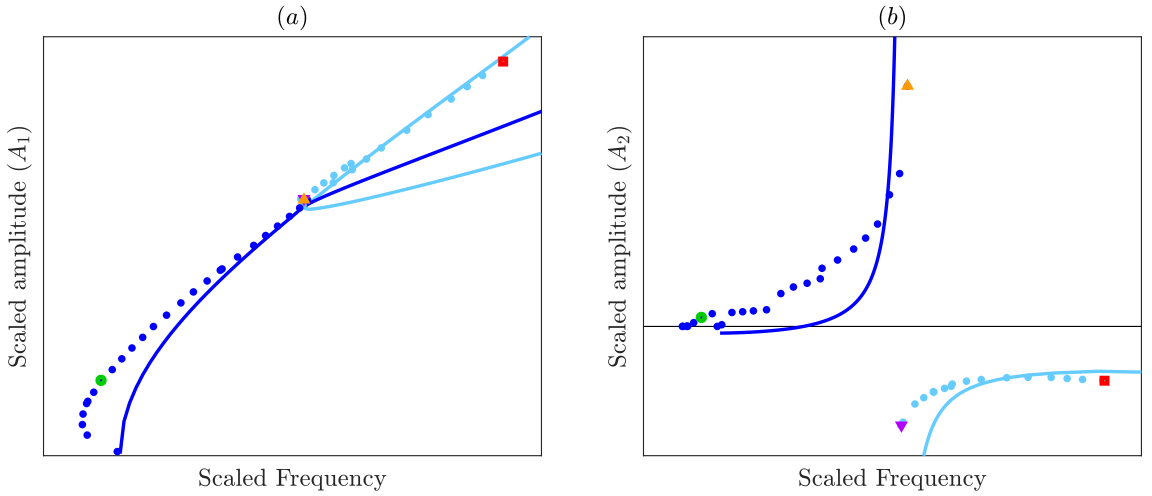

Fig. 7. A comparison between the experimentally-measured NNMs (previously shown in Fig. 6) and the NNM branches of the asymmetric ROM (previously shown in Fig. 5). Panel (*a*) is in the projection of the response frequency against the amplitude of acceleration of the first mode, A_1. Similarly, panel (*b*) is in the projection of the response frequency against amplitude of acceleration of the second mode, A_2. These frequencies and amplitudes have been scaled to allow for comparison between the model and the experiment.

at slightly different distances from the centre line of the beam. As a result, the beam is qualitatively similar to the asymmetric structure considered previously in Section 3.

4.2. Experimental results

Nonlinear normal modes represent the periodic responses of an unforced and undamped structure. Although the damping in the structure under consideration is light, its presence prevents an NNM motion from being reached precisely [30]. For the structure to exhibit a response that is close to that of an NNM, the forcing must negate the damping – a method known as force appropriation [22,31]. This is achieved by tuning the excitation force until it is in quadrature with the response (either displacement or acceleration). Here, force appropriation is performed using a single shaker and multiple excitation frequencies, where the excitation amplitudes are tuned manually with respect to the phase of the input force and two accelerometers (near the root and on the cross beam) [22]. Once this is achieved for one excitation frequency, and the response is recorded, the excitation frequency is adjusted, and the process is repeated.

Fig. 6 shows the results of the experimental measurements of the NNM branches using force appropriation. This is achieved by tuning the first and third harmonics of the force such that they are in quadrature with the corresponding harmonics of the displacement, to within 5° [22]. Panels (*a*) and (*b*) show the branches in the projection of the normalised response frequency against the amplitude of acceleration. In this case, the amplitude of acceleration represents the Fourier coefficient with the largest amplitude, and the response frequency corresponds to the frequency of this coefficient. For the first mode, the response frequency is normalised to the first linear natural frequency, ω_{n1}, and for the second mode the response frequency is normalised to three times the first linear natural frequency, $3\omega_{n1}$. In keeping with previous figures, the acceleration amplitudes in Fig. 6(*b*) have been adjusted to illustrate the phase between the modal accelerations – i.e. the light-blue, antiphase, NNM branch has a negative acceleration amplitude. The phase between the modes is also shown in Fig. 6(*c*–*f*), which illustrate that the modes are in antiphase for the responses represented by the purple triangle and red dot.

Initially, at low amplitudes, the experimentally-measured NNMs follow the lower portion of the primary branch, with one point on this branch marked with a green dot in Fig. 6. This is analogous to the response highlighted with a green dot in Fig. 5. Note that, at these low amplitudes, the NNM branch appears to soften before exhibiting a hardening behaviour. A similar phenomenon has been observed by Londoño et al. [32], and reported to be due to the effects of dry friction. At a higher frequency, the response transitions from the lower to the upper portion of the primary branch (denoted by an orange triangle). Again, this corresponds to the orange triangle in Fig. 5. As the frequency is increased, the sign of the forcing of the third harmonic is reversed, and the response then jumps from the upper portion of the primary branch to the lower portion of the isolated branch (denoted by a purple triangle). Note that, as with previous figures, this branch does not appear to be isolated when viewed in the projection of the first modal coordinate; however, the second modal coordinate clearly shows that this branch is isolated and responding with a different phase. At higher frequencies, the responses then follow the upper portion of the isolated branch (red square).

The transition from the primary to the isolated response branch does not require any specific change to the excitation applied to the system, but rather it is a *natural* behaviour. Whilst it may seem counter-intuitive that a response should *jump* from one NNM branch to another, it is to be expected if the phase-locking conditions of the NNM branches are considered. As discussed

previously, in Section 2.3, the phase-locking in the upper portion of the primary branch, and the lower portion of the isolated branch, is anticipated to be weak. As such, the forced response is not expected to follow these portions of the branch,[6] as observed in the experiment. This illustrates the importance of this isolated NNM branch, as it represents behaviour that is highly-likely to be observed when the system is forced.

There is a clear qualitative similarity between the NNM branches of the experimental system, in Fig. 6, and those of the asymmetric ROM, shown in Fig. 5. As discussed in Section 3.1, the finite-element model has not been updated to quantitatively match the experimental results. As such, to compare the numerical and experimental NNM branches, the experimentally-measured NNMs are scaled and superimposed in Fig. 7. This figure further highlights the similarity between these branches and confirms that the antiphase NNMs belong to an isolated branch.

5. Conclusions

Nonlinear normal modes are an important tool for understanding the dynamics of nonlinear systems, and for finding isolated forced response branches. However, in this paper, it has been shown that NNM branches may, themselves, be isolated. This has been illustrated using both a simple two-mode system, representative of an asymmetric physical system, and a nonlinear reduced-order model of a continuous cross-beam structure. The isolated NNM branches have also been observed experimentally in the cross-beam structure. In both systems, it has been shown that the isolated NNM branches may evolve from bifurcated branches by varying the physical parameters of the system. In the cross-beam structure, this evolution is driven by a breaking of the symmetry of the physical system; whilst the simple, two-mode system shows that a similar evolution may also occur in an asymmetric system.

As NNM branches are often computed using numerical continuation methods, isolated NNM branches pose a significant challenge as, without *a priori* knowledge of their existence, these branches may not be computed. Here, this problem is resolved by first computing the NNM branches using an analytical technique, which is unaffected by the isolated nature of the branches. The isolated NNM branches may correspond to significant responses when the system is forced; for example, in the cross-beam structure, the isolated branch was found to attract forced responses more strongly than the high-amplitude NNMs of the primary branch. This can be understood by considering the strength of the phase-locking in the NNMs of these branches.

Acknowledgements

The authors gratefully acknowledge the support of the Engineering and Physical Sciences Research Council who funded this work via S.A. Neild's Fellowship EP/K005375/1. The data presented in this work are openly available at 10.5281/zenodo.3243533.

Appendix A. Derivation of modal equations of motion using Lagrange's equation

The Lagrangian of the two-mode system may be written

$$\mathcal{L} = \left[\frac{1}{2}\dot{q}_1^2 + \frac{1}{2}\dot{q}_2^2\right] - \left[\frac{1}{2}\omega_1^2 q_1^2 + \frac{1}{2}\omega_2^2 q_2^2 + \frac{1}{4}\gamma_1 q_1^4 + \gamma_2 q_1^3 q_2 + \frac{1}{2}\gamma_3 q_1^2 q_2^2 + \gamma_4 q_1 q_2^3 + \frac{1}{4}\gamma_5 q_2^4\right], \tag{A.1}$$

where the terms in the first and second brackets represent the kinetic and potential energies of the system respectively. Applying the Euler-Lagrange equation, i.e.

$$\frac{\mathrm{d}}{\mathrm{d}t}\left(\frac{\partial \mathcal{L}}{\partial \dot{q}_i}\right) - \frac{\partial \mathcal{L}}{\partial q_i} = 0, \tag{A.2}$$

for each mode then gives

$$\ddot{q}_1 + \omega_1^2 q_1 + \gamma_1 q_1^3 + 3\gamma_2 q_1^2 q_2 + \gamma_3 q_1 q_2^2 + \gamma_4 q_2^3 = 0, \tag{A3a}$$

$$\ddot{q}_2 + \omega_2^2 q_2 + \gamma_2 q_1^3 + \gamma_3 q_1^2 q_2 + 3\gamma_4 q_1 q_2^2 + \gamma_5 q_2^3 = 0. \tag{A3b}$$

Note that the nonlinear parameters γ_2, γ_3 and γ_4 appear in both equations.

Appendix B. Modal equations of motion of a two-mass oscillator

The conservative, two-mass oscillator considered here consists of two equal masses, with mass m, connected by a spring, and both grounded by springs. These springs are all nonlinear, and have a restoring force given by $f_i = k_i\delta + \alpha_i\delta^3$, where δ is the extension of the spring. The spring grounding the first mass is denoted $i = 1$, the spring connecting the masses is denoted

[6] Note that this is not necessarily related to the stability of the NNM branch – it has been determined that the primary NNM branch of the ROM is stable throughout the region shown here, suggesting that the forced response does not jump from the primary branch due to a loss of stability.

$i = 2$ and the spring grounding the second mass is denoted $i = 3$. The equations of motion of this system may be written in the general form

$$\mathbf{M}\ddot{\mathbf{x}} + \mathbf{K}\mathbf{x} + \mathbf{N}_x(\mathbf{x}) = \mathbf{0}\,, \tag{B.1}$$

where $\mathbf{M}$ and $\mathbf{K}$ are the mass and stiffness matrices, respectively, $\mathbf{N}_x$ is a vector of nonlinear forces, and $\mathbf{x}$ is a vector of displacements, where

$$\begin{aligned} \mathbf{M} &= \begin{bmatrix} m & 0 \\ 0 & m \end{bmatrix}, \quad \mathbf{K} = \begin{bmatrix} k_1 + k_2 & -k_2 \\ -k_2 & k_2 + k_3 \end{bmatrix}, \\ \mathbf{x} &= \begin{bmatrix} x_1 \\ x_2 \end{bmatrix}, \qquad \mathbf{N}_x = \begin{bmatrix} \alpha_1 x_1^3 + \alpha_2 (x_1 - x_2)^3 \\ \alpha_2 (x_2 - x_1)^3 + \alpha_3 x_2^3 \end{bmatrix}. \end{aligned} \tag{B.2}$$

The parameter values considered here are given in Table B.4.

Table B.4
Physical parameters of the two-mass oscillator with nonlinear springs.

m[kg]	k_1 [Nm^{-1}]	k_2	k_3	α_1 [Nm^{-3}]	α_2	α_3
1	1	0.05	0.05	0.4	0.02	0.2

Eq. (B.1) is transformed from physical coordinates, $\mathbf{x}$, to modal coordinates, $\mathbf{q}$, using the linear modal transform $\mathbf{x} = \mathbf{\Phi}\mathbf{q}$, where $\mathbf{\Phi}$ is the modeshape matrix. For the physical parameters listed in Table B.4, the mass-normalised modeshape matrix is

$$\mathbf{\Phi} = \begin{bmatrix} -0.05241 & -0.9986 \\ -0.99863 & 0.05241 \end{bmatrix}. \tag{B.3}$$

Applying the linear modal transform leads to the modal equation of motion

$$\ddot{\mathbf{q}} + \mathbf{\Lambda}\mathbf{q} + \mathbf{N}_q(\mathbf{q}) = \mathbf{0}\,, \tag{B.4}$$

with

$$\mathbf{\Lambda} = \begin{bmatrix} \omega_1^2 & 0 \\ 0 & \omega_2^2 \end{bmatrix}, \qquad \mathbf{N}_q = \begin{bmatrix} \gamma_1 q_1^3 + 3\gamma_2 q_1^2 q_2 + \gamma_3 q_1 q_2^2 + \gamma_4 q_2^3 \\ \gamma_2 q_1^3 + \gamma_3 q_1^2 q_2 + 3\gamma_4 q_1 q_2^2 + \gamma_5 q_2^3 \end{bmatrix}, \tag{B.5}$$

where the linear natural frequencies, ω_{ni}, and modal nonlinear parameters, γ_i, are given in the main text in Table 1.

Appendix C. Relating the physical and modal nonlinear parameters

From the linear modal transform – used in Appendix B to find the modal equation of motion, Eq. (1) – the nonlinear parameter γ_2 may be written in terms of the nonlinear spring-stiffness parameters α_1, α_2 and α_3

$$\gamma_2 = \left[1.438 \times 10^{-4}\right] \alpha_1 + [-0.8904]\, \alpha_2 + [-0.05220]\, \alpha_3\,, \tag{C.1}$$

where the coefficients in square-brackets are shown to an accuracy of four significant figures. Therefore, the parameters α_1, α_2 and α_3 may be selected such that $\gamma_2 = 0$ and a bifurcation occurs. Note that, as the coefficients in Eq. (C.1) are dependent on the modeshape matrix, $\mathbf{\Phi}$, the mass and linear stiffness parameters could also be varied to achieve $\gamma_2 = 0$. For simplicity, the physical parameters are fixed to those given in Table B.4, and only α_2 is varied such that $\gamma_2 = 0$ is reached when

$$\alpha_2 = \alpha_{2,B} = \frac{1.438 \times 10^{-4} \alpha_1 - 0.05220 \alpha_3}{0.8904} \approx -0.01166\,. \tag{C.2}$$

Note that $\alpha_{2,B}$ has been used to denote this value of α_2. The modal nonlinear parameters (which are a function of α_2) are listed in Table 2 in the main text.

Appendix D. Supplementary data

Supplementary data to this article can be found online at https://doi.org/10.1016/j.jsv.2019.06.006.

References

[1] A. Nayfeh, B. Balachandran, Applied Nonlinear Dynamics: Analytical, Computational and Experimental Methods, Wiley Series in Nonlinear Science, Wiley, 2008.
[2] L. Manevitch, A. Manevich, The Mechanics of Nonlinear Systems with Internal Resonances, World Scientific, 2005.
[3] R.J. Kuether, L. Renson, T. Detroux, C. Grappasonni, G. Kerschen, M.S. Allen, Nonlinear normal modes, modal interactions and isolated resonance curves, J. Sound Vib. 351 (2015) 299–310, https://doi.org/10.1016/j.jsv.2015.04.035.
[4] A. Papangelo, F. Fontanela, A. Grolet, M. Ciavarella, N. Hoffmann, Multistability and localization in forced cyclic symmetric structures modelled by weakly-coupled duffing oscillators, J. Sound Vib. 440 (2019) 202–211.
[5] J.-P. Nol, T. Detroux, L. Masset, G. Kerschen, L. Virgin, Isolated response curves in a base-excited, two-degree-of-freedom, nonlinear system, in: ASME 2015 International Design Engineering Technical Conferences and Computers and Information in Engineering Conference, American Society of Mechanical Engineers, 2015, https://doi.org/10.1115/DETC2015-46106.
[6] G. Gatti, M.J. Brennan, Inner detached frequency response curves: an experimental study, J. Sound Vib. 396 (2017) 246–254, https://doi.org/10.1016/j.jsv.2017.02.008.
[7] A.D. Shaw, T.L. Hill, S.A. Neild, M.I. Friswell, Periodic responses of a structure with 3:1 internal resonance, Mech. Syst. Signal Process. 81 (2016) 19–34, https://doi.org/10.1016/j.ymssp.2016.03.008.
[8] N.A. Alexander, F. Schilder, Exploring the performance of a nonlinear tuned mass damper, J. Sound Vib. 319 (12) (2009) 445–462, https://doi.org/10.1016/j.jsv.2008.05.018.
[9] R.M. Rosenberg, Normal modes of nonlinear dual-mode systems, J. Appl. Mech. 27 (2) (1960) 263–268, https://doi.org/10.1115/1.3643948.
[10] A.F. Vakakis, Non-linear normal modes (NNMs) and their applications in vibration theory: an overview, Mech. Syst. Signal Process. 11 (1) (1997) 3–22, https://doi.org/10.1006/mssp.1996.9999.
[11] G. Kerschen, M. Peeters, J.C. Golinval, A.F. Vakakis, Nonlinear normal modes, part I: a useful framework for the structural dynamicist, Mech. Syst. Signal Process. 23 (1) (2009) 170–194, https://doi.org/10.1016/j.ymssp.2008.04.002 Special Issue: Non-linear Structural Dynamics.
[12] G. Haller, S. Ponsioen, Nonlinear normal modes and spectral submanifolds: existence, uniqueness and use in model reduction, Nonlinear Dynam. (2016) 1–42, https://doi.org/10.1007/s11071-016-2974-z.
[13] S. Bellizzi, R. Bouc, A new formulation for the existence and calculation of nonlinear normal modes, J. Sound Vib. 287 (3) (2005) 545–569.
[14] T.L. Hill, A. Cammarano, S.A. Neild, D.J. Wagg, Interpreting the forced responses of a two-degree-of-freedom nonlinear oscillator using backbone curves, J. Sound Vib. 349 (2015) 276–288, https://doi.org/10.1016/j.jsv.2015.03.030.
[15] T.L. Hill, S.A. Neild, A. Cammarano, An analytical approach for detecting isolated periodic solution branches in weakly nonlinear structures, J. Sound Vib. 379 (2016) 150–165, https://doi.org/10.1016/j.jsv.2016.05.030.
[16] S. Shaw, C. Pierre, Non-linear normal modes and invariant manifolds, J. Sound Vib. 150 (1) (1991) 170–173, https://doi.org/10.1016/0022-460X(91)90412-D.
[17] S. Shaw, C. Pierre, Normal modes for non-linear vibratory systems, J. Sound Vib. 164 (1) (1993) 85–124, https://doi.org/10.1006/jsvi.1993.1198.
[18] D.A. Ehrhardt, T.L. Hill, S.A. Neild, J.E. Cooper, Veering and nonlinear interactions of a clamped beam in bending and torsion, J. Sound Vib. 416 (2018) 1–16, https://doi.org/10.1016/j.jsv.2017.11.045.
[19] M.P. Mignolet, A. Przekop, S.A. Rizzi, S.M. Spottswood, A review of indirect/non-intrusive reduced order modeling of nonlinear geometric structures, J. Sound Vib. 332 (10) (2013) 2437–2460.
[20] R.W. Gordon, J.J. Hollkamp, Reduced-order Models for Acoustic Response Prediction, Tech. Rep. AFRL-RB-WP-TR-2011-3040, Air force research laboratory, 2011.
[21] J.J. Hollkamp, R.W. Gordon, Reduced-order models for nonlinear response prediction: implicit condensation and expansion, J. Sound Vib. 318 (45) (2008) 1139–1153.
[22] D.A. Ehrhardt, M.S. Allen, Measurement of nonlinear normal modes using multi-harmonic stepped force appropriation and free decay, Mech. Syst. Signal Process. 7677 (2016) 612–633, https://doi.org/10.1016/j.ymssp.2016.02.063.
[23] T.L. Hill, A. Cammarano, S.A. Neild, D.J. Wagg, Out-of-unison resonance in weakly nonlinear coupled oscillators, Proc. R. Soc. Lond.: Math., Phys. Eng. Sci. 471 (2014) 2173, https://doi.org/10.1098/rspa.2014.0659.
[24] K. Ikeda, K. Murota, Imperfect Bifurcation in Structures and Materials: Engineering Use of Group-Theoretic Bifurcation Theory, Applied Mathematical Sciences, Springer, New York, 2002.
[25] T.L. Hill, S.A. Neild, A. Cammarano, D.J. Wagg, The influence of phase-locking on internal resonance from a nonlinear normal mode perspective, J. Sound Vib. 379 (2016) 135–149, https://doi.org/10.1016/j.jsv.2016.05.028.
[26] T.L. Hill, A. Cammarano, S.A. Neild, D.A.W. Barton, Identifying the significance of nonlinear normal modes, Proc. Roy. Soc. Lond.: Math., Phys. Eng. Sci. 473 (2199) (2017), https://doi.org/10.1098/rspa.2016.0789.
[27] Dassault Systmes, ABAQUS Documentation, Providence, RI, USA, 2017.
[28] M. Peeters, R. Vigui, G. Srandour, G. Kerschen, J.-C. Golinval, Nonlinear normal modes, part II: toward a practical computation using numerical continuation techniques, Mech. Syst. Signal Process. 23 (1) (2009) 195–216, https://doi.org/10.1016/j.ymssp.2008.04.003 special Issue: Non-linear Structural Dynamics.
[29] A. Cammarano, T.L. Hill, S.A. Neild, D.J. Wagg, Bifurcations of backbone curves for systems of coupled nonlinear two mass oscillator, Nonlinear Dynam. 77 (12) (2014) 311–320, https://doi.org/10.1007/s11071-014-1295-3.
[30] L. Renson, T.L. Hill, D.A. Ehrhardt, D.A.W. Barton, S.A. Neild, Force appropriation of nonlinear structures, Proc. Roy. Soc. Lond.: Math., Phys. Eng. Sci. 474 (2018) 2214, https://doi.org/10.1098/rspa.2017.0880.
[31] M. Peeters, G. Kerschen, J. Golinval, Modal testing of nonlinear vibrating structures based on nonlinear normal modes: experimental demonstration, Mech. Syst. Signal Process. 25 (4) (2011) 1227–1247, https://doi.org/10.1016/j.ymssp.2010.11.006.
[32] J.M. Londoo, S.A. Neild, J.E. Cooper, Identification of backbone curves of nonlinear systems from resonance decay responses, J. Sound Vib. 348 (2015) 224–238, https://doi.org/10.1016/j.jsv.2015.03.015.